AIAA JOURNAL
Vol. 38, No. 7, July 2000

Velocity Measurements in a Shock-Separated Free Shear Layer

C. W. Palko* and J. C. Dutton†
University of Illinois at Urbana–Champaign, Urbana, Illinois 61801

Two-component laser Doppler velocimetry measurements were made in a planar, shock-separated free shear layer formed by the convergence of two supersonic streams past a thick plate. High-speed wall-pressure measurements were used to locate the unsteady shock wave formed by this interaction and, consequently, facilitated separation of the effects of shock motion from the turbulent fluctuations in the velocity measurements of the shear layer. Shock-induced flow separation dramatically increases the turbulent normal and shear stresses. The shock-separated shear layer displays a positive shear stress region between separation and reattachment. Reattachment produces a shift in turbulent kinetic energy from the streamwise component to the transverse component. The region of shock motion has a relatively constant width, irrespective of distance from the wall.

Nomenclature

a = speed of sound
C_f = skin-friction coefficient
M = Mach number
M_C = convective Mach number
P = pressure
Re = Reynolds number
U = mean streamwise velocity
U_∞ = freestream velocity
u = instantaneous streamwise velocity
u_τ = friction velocity
V = mean transverse velocity
v = instantaneous transverse velocity
X, Y = flowfield streamwise and transverse coordinates
δ = shear-layer or boundary-layer thickness
δ^* = boundary-layer displacement thickness
θ = boundary-layer momentum thickness
Π = wake strength factor
$\langle\ \rangle$ = ensemble averaged

Subscripts

δ = shear-layer or boundary-layer thickness
δ^* = boundary-layer displacement thickness
θ = boundary-layer momentum thickness
1, 2 = high-speed and low-speed, respectively, or upper and lower streams, respectively

Superscript

$'$ = fluctuation from the mean

Introduction

FLOWFIELDS involving shock-induced boundary-layer separation are important and widespread. This study represents one such flow called plume-induced boundary-layer separation (PIBLS). PIBLS can occur on any supersonic vehicle with an underexpanded exhaust plume including aircraft, rockets, and missiles. One famous case of PIBLS is on the Saturn V first stage, where PIBLS appeared to play a dominant role in base-heating and base-burning phenomena.[1,2] Although shock-induced boundary-layer separation caused by a second fluid stream has been investigated over the last 40 years, there are no known turbulence measurements of such a flow. However, shock-induced shear-layer formation in front of solid objects has been investigated.[3–6] Among these geometries, unswept compression corner flows provide the closest analogy to the current study.

To date only four studies of turbulence in unswept compression corners have been performed: Ardonceau,[7] Kuntz,[8] Smits and Muck,[9] and Selig et al.[10] All of the studies, except for that of Selig et al., considered a series of corner angles resulting in both unseparated and separated flows. Unlike the other studies, Selig et al. investigated a flowfield with active forcing (by mass addition). All of Kuntz's[8] data and some of Ardonceau's[7] were obtained using two-component laser Doppler velocimetry (LDV). The remaining studies, including a portion of Ardonceau's, used constant temperature hot-wire anemometry. The Mach numbers for the studies by Ardonceau,[7] Kuntz,[8] Smits and Muck,[9] and Selig et al.[10] were 2.25, 2.94, 2.90, and 2.84, respectively. All of these studies noted large increases in turbulence through the shock interaction and unsteady shock motion. However, none of these studies used any conditional analysis to separate velocity fluctuations due to the motion of the shock from those due to turbulence. Palko and Dutton[11] have demonstrated a technique for separating the fluctuation contributions from these two sources; this method is used in the measurements reported here.

Several mechanisms have been proposed to explain the turbulence amplification in shock wave/boundary-layer interactions. A nonlinear coupling of entropy, pressure, and vorticity fluctuations involving the Rankine–Hugoniot jump conditions at the shock has been proposed by Anyiwo and Bushnell.[12] Turbulence amplification as a direct result of shock wave unsteadiness[13,14] is also widely cited. Finally, both bulk compression and concave streamline curvature present in shock wave/boundary-layer interactions are known to be destabilizing and, therefore, turbulence enhancing.[15] All four of these mechanisms become more significant as the corner angle is increased, thereby increasing the shock strength and the range of shock motion. Another mechanism that is not often cited is the effect of flow separation itself.

The studies of Ardonceau,[7] Kuntz,[8] Smits and Muck,[9] and Selig et al.[10] all involved relatively thick boundary layers (8, 8, 26, and 26 mm, respectively) and very small separated regions. The current study involves an approximately 3-mm-thick turbulent incoming boundary layer and a large separated flow region. This separation bubble serves as a reservoir of low-momentum fluid that may be entrained by turbulent structures within the free shear layer. Unfortunately, the lack of previous studies involving a large separated region makes the effects of separation caused by a second fluid stream rather than by a solid ramp face difficult to determine.

In contrast to the case of shock-separated free shear layers are expansion-separated shear layers. To help understand the flow physics of the shock-separated case, this paper will make comparisons with the work of Amatucci[16] and Herrin,[17] which represents

Presented as Paper 98-0698 at the AIAA 36th Aerospace Sciences Meeting, Reno, NV, 12–15 January 1998; received 16 May 1998; revision received 13 August 1999; accepted for publication 13 August 1999.

*National Defense Science and Engineering Graduate Fellow, Department of Mechanical and Industrial Engineering; currently Senior Member of the Technical Staff, Vehicle Concepts Department, The Aerospace Corporation, El Segundo, CA 90245. Member AIAA.

†W. Grafton and Lillian B. Wilkins Professor, Department of Mechanical and Industrial Engineering, Room 140, Mechanical Engineering Building, MC-244; j-dutton@uiuc.edu. Associate Fellow AIAA.

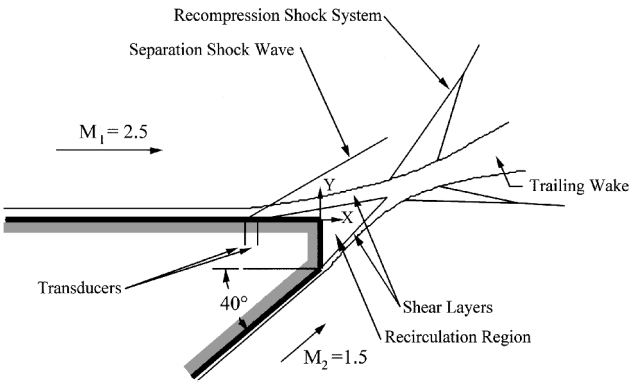

Fig. 1 Planar flowfield schematic, 50.8 mm wide.

comprehensive LDV investigations of the mean flow and turbulence in planar and axisymmetric expansion-separatedshear layers, respectively. Herrin investigated a single $M = 2.5$ (before separation) shear layer, whereas Amatucci[16] studied both $M = 2.56$ and 2.05 shear layers. Similar to the current study, both Amatucci's and Herrin's[17] flows involved relatively thin incoming boundary layers and a large separated flow region.

Flow Facility

A schematic diagram of the 50.8-mm-wide planar test section, with the flowfield features investigated in this study, is shown in Fig. 1. The upper Mach 2.5 stream (unit Reynolds number, unit $Re = 48.9 \times 10^6$ m^{-1}) and the lower Mach 1.5 stream (unit $Re = 36.2 \times 10^6$ m^{-1}) converge at a 40-deg angle past a 12.7-mm-high base plane. (The unit Reynolds number is defined using the mean velocity and temperature-corrected viscosity of each freestream. A length scale is not chosen due to the lack of a single obviously correct dimension, hence the units of inverse meters.) The boundary layer of the upper stream intercepts the oblique separation shock, consequently separates, and forms a free shear layer, as shown in Fig. 1. This shear layer then reattaches with the shear layer formed by the separation (at a nearly zero pressure gradient) of the boundary layer of the lower stream, thereby enclosing a recirculating region behind the base. The reattachment of the shear layers generates a recompression shock system and the resulting trailing wake.

The upper and lower streams have absolute stagnation pressures of 506 and 251 kPa, respectively, resulting in a static pressure ratio of the lower to the upper streams of $P_2/P_1 = 2.27$. With this pressure ratio, the wind tunnel has a run time of approximately 5 min. Honeycomb and fine mesh screens are installed in both streams (upstream of the converging–diverging nozzles) to reduce turbulence in the incoming flow. The resulting freestream turbulence is very low in both streams, for example, in the upper stream, $\langle u'^2 \rangle < 0.0005 U_\infty^2$. Surface oil flow visualization shows that the center 32 mm (63%) of the flowfield is free from sidewall effects and is, consequently, two dimensional in this region. The blowdown-type supersonic wind tunnel used to produce this flowfield is described briefly by Palko and Dutton[11] and comprehensively by Palko[18] and Shaw.[19]

Equipment

A two-component LDV system, with a TSI IFA 750 digital burst correlator operating in coincident mode, was used for the mean velocity and turbulence measurements. The IFA 750 includes sophisticated internal filters that greatly reduce the impact of electronic noise from the photomultiplier tubes. The IFA 750 has been shown, at the University of Illinois Gas Dynamics Laboratory and elsewhere, to be far less sensitive to electronic noise than the older-style counters previously used for LDV measurements. A detailed discussion of the IFA 750 operation is given by Jenson.[20] One beam of each color is shifted by 40 MHz to minimize fringe biasing and to allow discrimination of negative velocities. The blue and green beam pairs are also oriented at approximately +45 and −45 deg, respectively, to the mean flow direction of the upper stream to minimize fringe blindness. An LDV coincident time window of 20 μs was selected by using a rule of thumb suggested by TSI, Inc., the LDV system manufacturer. The window was selected to be $\frac{1}{10}$th the time between data (obtained from the inverse of a representative data rate for this study, i.e., 5000 Hz).

Separate TSI model 9306 six-jet atomizers introduce silicone oil droplets with a mean diameter of approximately 0.8 μm into each stream.[21] The oil droplets are injected downstream of all flow-conditioning modules and upstream of the nozzle blocks through small stainless steel tubes. The scattered light from the droplets is collected in forward scatter at an off-axis collection angle of 10 deg, resulting in an effective coincident measurement volume length of 1.5 mm. The 13-mm beam spacing and 250-mm focal length transmitting lens result in a coincident measurement volume diameter of 0.127 mm (the spatial resolution in the two velocity measurement directions). To minimize the effects of seed particle concentration bias in the reported data, the seeding levels were adjusted in each stream to yield the same scattered light intensity. After this adjustment was completed, traverses were made through the shear layer while seeding one or both streams. The results agreed closely for both mean and rms velocities.[18]

Because of their significant inertia, seed particles produce curved pathlines behind an oblique shock wave instead of following the fluid streamlines that bend discontinuously at the shock front. Using the Carlson–Hoglund[22] empirical drag law, significant particle lag effects in this study were estimated to be limited to a region extending 2.8 mm in the streamwise X direction downstream of the shock wave, that is, 1.4 mm normal to the shock. This oblique shock wave represents by far the largest velocity gradient in the present flowfield.

The worst-case Stokes number of the seed particles was calculated to be 0.3 for the region outside the noted particle lag region immediately downstream of the shock wave. This worst-case Stokes number occurs just downstream of separation where the shear layer is the thinnest. The simulations of Samimy and Lele[23] indicate that a Stokes number of 0.3 would result in an rms velocity error of 3%. However, Samimy and Lele's study used a convective Mach number of 0.6, whereas the region of the present flow with the largest Stokes number has a convective Mach number greater than 1.4. As discussed by Smith,[24] increased compressibility (indicated by a larger convective Mach number) reduces the shear-layer growth rate and inhibits turbulent mixing. Thus, the particle lag errors in the present study are expected to be significantly less than the 3% predicted by Samimy and Lele.[23]

Because the boundary-layer separation point oscillates in the streamwise direction with the shock wave, the shear layer will also oscillate and cause biasing of unconditionally averaged velocity data. Palko and Dutton[11] and Palko[18] describe in detail the conditional analysis technique used in the current study to minimize bias in the velocity measurements due to shock wave unsteadiness. This technique allows the shock position (upstream, between, or downstream of the two transducers) to be determined for each velocity realization. By ensemble-averaging realizations that are obtained only when the shock is between the transducers, this procedure effectively freezes the shock position and minimizes the velocity fluctuations that would otherwise be recorded due to shock motion. However, large data sets must be obtained to ensure adequate statistical certainty from the ensemble averages. Because the transducers are placed 19.0 and 16.5 mm upstream of the base plane (Fig. 1), the mean shock foot position, that is, the boundary-layer separation point, for the conditionally analyzed data set is 17.75 ± 1.6 mm upstream of the base, where the transducer diameter is 1.6 mm. Palko[18] describes in detail the entire pressure data acquisition system.

Palko[18] includes a comprehensive uncertainty analysis including consideration of fringe, velocity, particle concentration, velocity gradient, and particle dynamics biases, as well as measurement volume positional uncertainty and overall optical measurement uncertainty (primarily in fringe spacing). The systematic or bias errors are conservatively estimated to be less than 2% for the mean velocities and 4% for the normal stresses. As noted in Ref. 25, accurate estimates of the uncertainty in heterogeneous statistical moments such as shear stress require detailed knowledge of the relationships between the variables. Obviously, this knowledge does not exist in complex flows such as the current one. The authors believe that

the systematic error in the shear stress should be of the same order of magnitude as for the normal stresses and that a more specific estimate could be misleading.

The 95% confidence interval for the random error in the normal stresses is (−4.3%, +4.6%) of the measured value for each normal stress. The 95% confidence interval for the random error in the mean velocity is (−3.1%, +3.1%) of the standard deviation in the measured velocity. The error in the mean streamwise velocity U at the point with the largest standard deviation is ±3.3% ($U = 177 \pm 5.9$ m/s). For comparison, at reattachment (where the mean velocity is zero), the random error in U is only ±2.6 m/s, although the percentage error is extremely large (division by nearly zero). For the transverse mean velocity V, the random error corresponding to the point of largest standard deviation is ±7.5% ($V = 29.5 \pm 2.2$ m/s), whereas the error at reattachment is only ±2.5 m/s, although once again the percentage error is quite large.

Results

This paper presents data obtained at approximately 1500 spatial locations along the spanwise centerplane of the flowfield. The origin of the measurement grid is the upper base corner with the X axis aligned parallel to the wall (Fig. 1). Although some related studies, most notably by Kuntz[8] and Amatucci,[16] used a coordinate system rotated to align with the local mean velocity along the shear layer, these studies were of much larger scale flows, with widely separated shear layers, and present the data as line profiles. The current flowfield is much smaller in scale, making the use of numerous rotated coordinate systems impractical. Instead, a single orthogonal coordinate system for which streamwise refers to the X coordinate (perpendicular to the base plane) and transverse refers to the Y coordinate (parallel to the base plane) has been used. This allows the presentation of data as contour plots covering the entire flowfield. Despite this difference in coordinate systems, comparisons to previous studies remain useful. The streamwise spacing of the measurement locations is a uniform 2.5 mm, but the transverse spacing varies from 0.125 mm in high-gradient regions to 1.0 mm in the almost uniform freestreams. Two-component velocity measurements are limited to $Y > 1$ mm (upstream of the upper base corner) due to beam clipping at the wall below this point. The entire measurement grid has an absolute positional uncertainty (systematic error) in the streamwise and transverse directions of $\pm 250\,\mu$m with respect to the base, but the relative positional uncertainty (random error) of each point with respect to each other within the measurement grid is only $\pm 0.5\,\mu$m.

Previously, Palko and Dutton[11] presented selected profiles obtained with and without conditional analysis to illustrate the effects of shock motion on the turbulence. The present paper instead analyzes global flowfield features by presenting results (using 4096 instantaneous velocity realizations at each spatial location) obtained only when the shock was between the two transducers. The contour levels in the data plots do not represent regular intervals in the data but instead were chosen to illustrate clearly the features of the flowfield. Furthermore, the mean velocities and Reynolds stresses have been nondimensionalized using the freestream velocity in the upper stream, $U_\infty = 590$ m/s. Finally, all contour and line plots presented in this study are unsmoothed, and the data have been velocity debiased using the interarrival time weighting method shown by Herrin and Dutton[26] to be the most accurate debiasing method in this type of flow.

Mean Flow

Table 1 lists various properties of the incoming boundary layer of the upper stream. These properties were determined by applying a curve fit for compressible, turbulent boundary layers[27] to the experimentally obtained boundary-layer profile. The best curve fit was found by varying the boundary-layer thickness δ and the skin-friction coefficient C_f until the mean square deviation between the curve fit and the experimental data was minimized. The resulting profile equation was then numerically integrated to yield the boundary-layer integral parameters listed in Table 1. The Reynolds numbers based on the various thicknesses may be estimated as $Re_\delta = 1.2 \times 10^5$, $Re_{\delta^*} = 2.8 \times 10^4$, and $Re_\theta = 7.6 \times 10^3$.

Table 1 Approach boundary-layer properties

Property	Value
Boundary-layer thickness δ, mm	3.2
Displacement thickness δ^*, mm	0.78
Momentum thickness θ, mm	0.21
Shape factor, $H = \delta^*/\theta$	3.7
Wake strength factor Π	0.86
Skin friction coefficient C_f	0.0016
Friction velocity u_τ, m/s	23.6

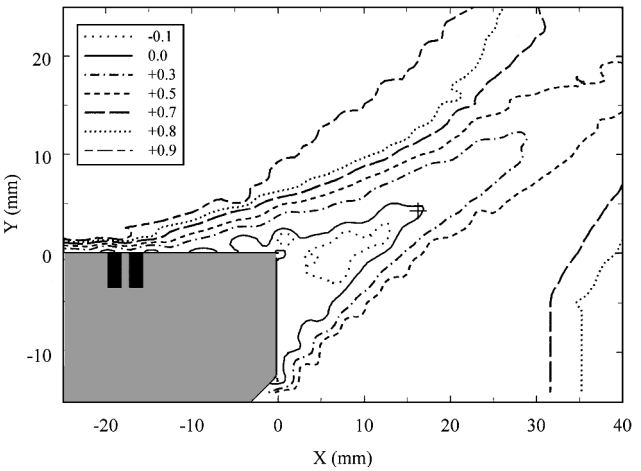

Fig. 2 Mean streamwise velocity field, U/U_∞.

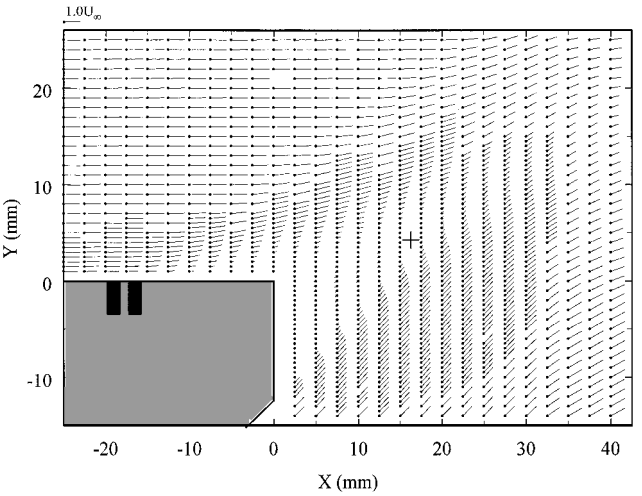

Fig. 3 Mean velocity vector field.

Figure 2 presents a contour plot of the normalized mean streamwise velocity component U/U_∞. These results clearly indicate the approach boundary layer, the two shear layers, the recirculation region behind the base (denoted by negative values of U/U_∞), the separation shock, the upper system of recompression waves, and the trailing wake. The two shear layers reattach at approximately 16.25 mm downstream of the base. (Because of the dominance of the streamwise velocity component, reattachment is defined here as the point of zero U/U_∞.) The reattachment point is noted by a small plus sign in Fig. 2 and all subsequent contour plots. Also interesting is the sudden, almost discontinuous decrease in the streamwise mean velocity and subsequent thickening of the boundary layer at the shock foot location ($X = -17.75$ mm). The presence of this discontinuity at the expected location between the two transducers indicates that the shock position is accurately frozen by the conditional analysis algorithm.

The combined mean velocity field (streamwise and transverse components) is presented as a vector plot in Fig. 3. Figure 3 clearly shows the uniform flow in each freestream approaching the base,

the two shear layers, the separation shock, the reattachment point at $X = +16.25$ mm, and the wake development. The thickening of the upper boundary layer as the base plane is approached is also apparent in Fig. 3. The inflection points in the velocity profiles immediately upstream of the base are expected because the flow is separated at these locations. To allow closer examination of the recirculation region, a vector plot of only the base region is presented in Fig. 4. The two distinct recirculating eddies within the region of separated flow may be clearly seen in Fig. 4, as well as the recirculating flow near the wall at the base plane below the upper shear layer. The reattachment of the two shear layers in the neighborhood of $X = +16$ mm is also more apparent in this expanded view.

An equivalent ramp corner angle may be defined for the current flow as the angle between the mean reattached wake direction (inviscid slip line) and the X axis. This inviscid slip line is, of course, a compliant boundary rather than a rigid boundary such as the downstream ramp surface in a compression corner. By using a linear regression through the points of minimum streamwise velocity at all measured streamwise locations downstream of reattachment, this equivalent corner angle is estimated to be 28 deg.

Figure 5 presents the mean Mach number distribution throughout the flowfield. The Mach number was obtained by measuring the stagnation temperature inside the plenum chamber of the wind tunnel using an iron–constantan thermocouple and by applying the assumption of adiabatic flow to extract the static temperature and speed of sound throughout the flowfield. Figure 5 clearly reveals the separation shock, the recompression wave systems, and the large subsonic region downstream of the base. The dramatic change in compressibility across the upper shear layer is indicated by the highly compressible freestream on the outside ($M > 2.0$) and the large region

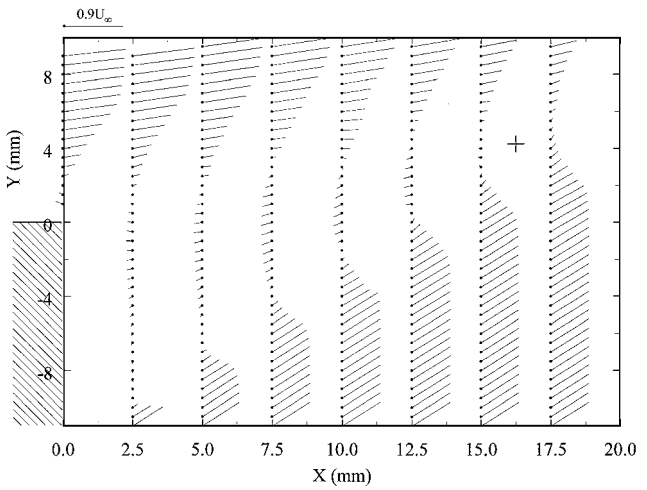

Fig. 4 Base region mean velocity vector field.

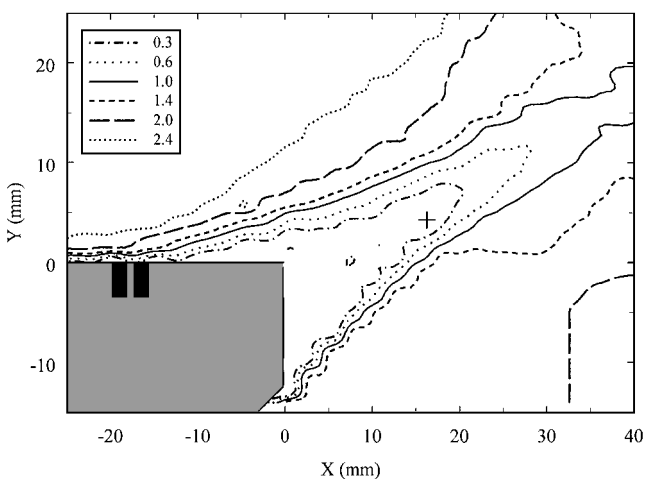

Fig. 5 Mean Mach number field.

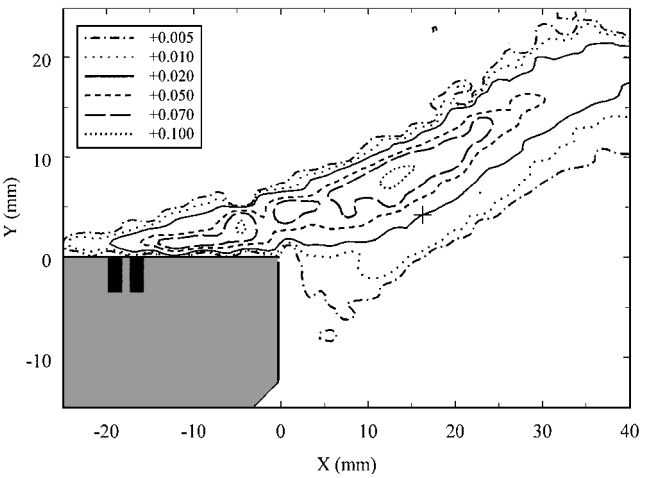

Fig. 6 Streamwise normal stress field, $\langle u'^2 \rangle / U_\infty^2$.

of nearly incompressible flow near the base on the inside of this thin layer ($M < 0.3$).

To quantify the compressibility of the shock-separated shear layer, one may use the mean velocity data to determine a convective Mach number M_C (Refs. 28 and 29). The convective Mach number is the Mach number of each freestream relative to the large-scale turbulent structures in the free shear layer. For cases in which the freestream gases on each side of the shear layer are the same and stream 1 is the high-speed stream, the convective Mach number can be computed as

$$M_C = (U_1 - U_2)/(a_1 + a_2) \tag{1}$$

For the upper shear layer in this study, the convective Mach number is approximately 1.4, which indicates very strong effects of compressibility. This value of M_C is also approximately equal to those of the planar and axisymmetric expansion-separated free shear layers in the studies of Amatucci[16] and Herrin,[17] respectively.

Reynolds Normal Stresses

The dimensionless streamwise normal stress distribution is shown in Fig. 6. Clearly, the turbulence in both freestreams is very small. The shock-induced separation process dramatically increases the streamwise normal stress, and the reattachment process and wake development dramatically decrease it in the upper shear layer. The shock interaction increases the streamwise normal stress by a factor of about 5.5 times the peak measured value in the incoming boundary layer of $0.02U_\infty^2$. The maximum streamwise normal stress value of $0.11U_\infty^2$ occurs immediately upstream of reattachment.

The increased streamwise turbulence levels in the current study match closely those cited by Ardonceau[7] in his separated, 18-deg compression corner flow, but exceed those cited in the other shock interaction studies. These differences could be attributable to possible difficulties in interpreting hot-wire measurements made in supersonic flows[9] and the lack of LDV data immediately downstream of the interaction in Kuntz's[8] study. The peak streamwise turbulence levels in the present study exceed those of both Herrin[17] and Amatucci.[16] This difference is due to the presence of the adverse pressure gradient, bulk compression, and concave streamline curvature at separation for the current shock-separated shear layer, as compared to the expansion-separated cases.

The transverse normal stress distribution is shown in Fig. 7. Separation of the upper shear layer dramatically increases the transverse normal stress by a factor of 5 over that in the incoming boundary layer. The lower shear layer displays large values of transverse normal stress, but this is primarily due to the inclination of the lower shear layer with respect to the X axis. Because of this, velocity fluctuations within the lower shear layer have a large transverse component. Note that the region of highest transverse velocity fluctuations occurs in the lower portion of the separated region. In this region the streamwise velocity fluctuations are between the 0.01 and 0.02 contours. Although not presented here, a normal stress

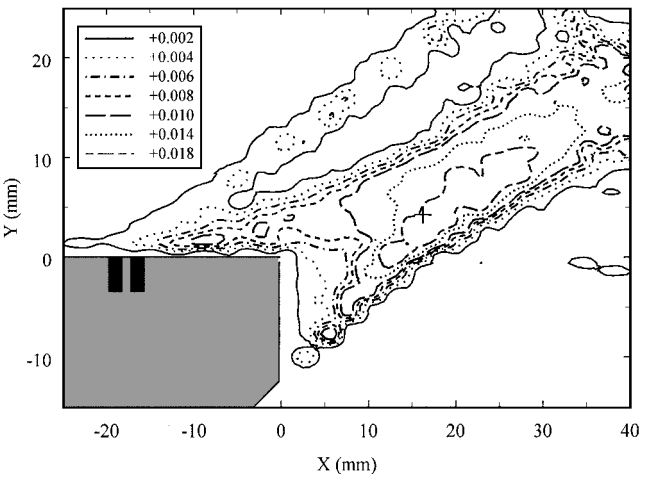

Fig. 7 Transverse normal stress field, $\langle v'^2 \rangle / U_\infty^2$.

anisotropy plot presented by Palko[18] reveals that the majority of the separated region has an anisotropy of less than 2. The region of very large streamwise velocity fluctuations (0.1 contour) occurs inside the upper shear layer.

Whereas the transverse normal stress in the lower shear layer (and for the entire flowfield) peaks before reattachment (at $X = +12.5$ mm), the transverse normal stress in the upper shear layer increases throughout the recompression region and through reattachment. In general the developing wake exhibits decreasing turbulence levels, but large values ($>0.018U_\infty^2$) of transverse normal stress persist for over 12.5 mm downstream of reattachment (to $X = +28.75$ mm). The far wake is characterized by decreasing transverse normal stress, but at the downstream limit of the measurement region ($X = +40$ mm), the values are still greater than $0.010U_\infty^2$ (which is equal to the value immediately after separation). This delayed decrease in the transverse normal stress may be indicative of a shift in turbulent energy with recompression and reattachment from the streamwise normal stress to the transverse and spanwise normal stresses. Herrin and Dutton[30] also note increasing normal stress isotropy through reattachment of an axisymmetric shear layer that is indicative of such a shift in turbulent energy. This delayed decrease may also be due to the large transverse normal stress in the lower shear layer that comes primarily from the inclination of the lower shear layer with respect to the X axis.

The streamwise normal stress in the current study peaks immediately before reattachment. This feature is common to compressible free shear layers formed through both planar rapid expansions[16] and planar shock-induced separation,[18] but contrasts with the decreasing turbulence levels through recompression and reattachment in axisymmetric geometries.[30] This provides evidence of the stabilizing, that is, turbulence-reducing effect of lateral streamline convergence for the axisymmetric case, which does not occur for the planar case.

Turbulence Amplification

Turbulence amplification has been documented in many types of shock wave/boundary-layer interactions. Smits and Muck[9] reported in their 8-, 16-, and 20-deg compression corner studies normal stress amplification factors of up to 14 times the incoming boundary-layer values, with the larger corner angles, that is, stronger shocks, exhibiting the larger turbulence amplification. Smits and Muck used the strong Reynolds analogy (SRA) to extract the kinematic turbulent stresses from the mass-weighted hot-wire measurements. However, the SRA assumes that pressure fluctuations are negligible, which is not true downstream of unsteady shock waves and, therefore, complicates the interpretation of hot-wire measurements in such flows. Kuntz[8] reported peak streamwise normal stress levels in the reattached boundary layer of between 2 and 10 times the levels in the approaching boundary layer, for his 8-, 12-, 16-, 20-, and 24-deg compression corners, respectively. Larger turbulence amplification factors may well have occurred in Kuntz's flow upstream of reattachment but were not measured. By comparison, the streamwise normal stress in the present study peaks upstream of reattachment. In his 18-deg compression corner, Ardonceau[7] reports a peak streamwise normal stress value just below the center of his shear layer prior to reattachment of $0.114U_\infty^2$, an increase of a factor of 4.3 over the approaching boundary-layer values. This agrees well with the peak value in the present study. The normal stress amplification ratios quoted for Kuntz[8] and Ardonceau[7] are estimated from turbulence intensity profiles and consequently have large uncertainties.

Ardonceau,[7] Kuntz,[8] and Smits and Muck[9] examined a range of compression corner angles. All of these studies found increasing turbulence amplification with increasing corner angle and attributed it to increasing shock strength, bulk compression, and concave streamline curvature. Both Ardonceau[7] and Kuntz[8] found no dramatic difference between separated (larger angles) and unseparated (smaller angles) corner flows, indicating that separation has little effect on turbulence amplification. Smits and Muck[9] concluded that for weak shocks turbulence amplification is primarily due to the effects of bulk compression, adverse pressure gradient, and concave streamline curvature. Smits and Muck assert that the turbulence amplification depends more on the overall pressure rise through the interaction than on the presence of a shock wave. They also proposed that shock wave oscillation becomes an important mechanism for stronger shocks.

Selig and Smits,[14] however, in a separated 24-deg compression corner study, concluded that shock unsteadiness is not an important mechanism because the downstream turbulence showed no change when the shock wave was driven at a particular frequency. The shock wave was forced in this flow by periodic blowing into the separated region, and unlike the present study, no conditional analysis was used to isolate either shock position or shock motion direction from the turbulent fluctuations. In contrast, Palko and Dutton[11] found that shock motion direction does have a significant effect on downstream turbulence levels as well as on the organization of the turbulence.

Amatucci[16] and Herrin[17] also report turbulence increases smaller than the earlier cited levels for their planar and axisymmetric base flows, respectively. Both researchers found that, despite the stabilizing influences of a favorable pressure gradient, bulk expansion, and convex streamline curvature, the turbulence at the inner (low-speed) edge of the free shear layer increases dramatically over its levels in the approaching boundary layer in response to the expansion at separation. In particular, Herrin found that the turbulence levels in the outer portion of his free shear layer formed through a rapid expansion were frozen at or below the upstream levels, whereas the inner edge experienced streamwise normal stress increases of approximately 9 times the levels in the approaching boundary layer.

Ardonceau[7] and Kuntz[8] report increases of 9 and 20, respectively, over the peak transverse normal stress levels in the approaching boundary layers for their compression corner flows. Herrin[17] reports a peak transverse normal stress value of $0.024U_\infty^2$ for his rapidly expanded axisymmetric free shear layer. The data of Herrin reflect an increase of 3 times the transverse normal stress level in his approaching boundary layer. Amatucci's[16] data display amplifications of roughly 3 and 8 times the peak transverse normal stress levels in the approaching boundary layers for his upper (Mach 2.56) and lower (Mach 2.05) rapidly expanded planar shear layers, respectively. The peak transverse normal stress amplification factor in the present study lies within the range cited earlier.

Turbulent Kinetic Energy

The turbulent kinetic energy (TKE) distribution (where the spanwise normal stress is assumed equal to the transverse normal stress) is shown in Fig. 8. The TKE contours resemble closely the streamwise normal stress contours (Fig. 6). The streamwise normal stress is much larger than its transverse counterpart over most of the flowfield and so dominates the TKE. Therefore, similar to the streamwise normal stress, the TKE is much larger in the upper shear layer than in the lower shear layer and peaks near reattachment.

Unlike the present study, both Kuntz[8] and Amatucci[16] approximated the spanwise normal stress as the average of the streamwise and transverse normal stresses. This average definition may overstate the actual value of the TKE. Herrin,[17] however, was able to measure all three velocity components and, therefore, determined the TKE without any approximations. The maximum TKE in the present

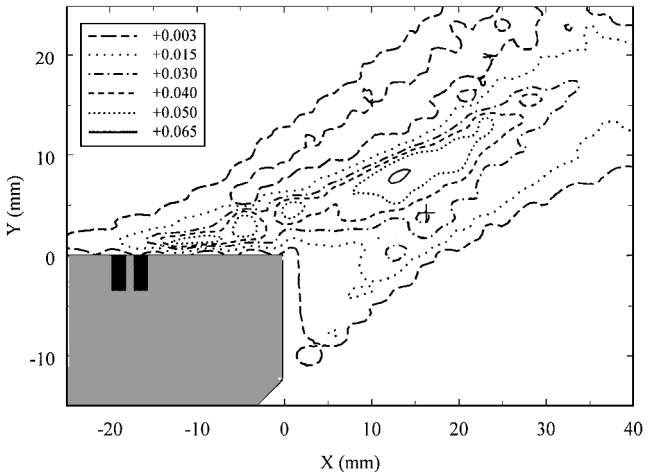

Fig. 8 TKE field, $(\langle u'^2 \rangle + 2\langle v'^2 \rangle)/2U_\infty^2$.

study, $0.07U_\infty^2$, exceeds the maximum value of $0.042U_\infty^2$ Herrin found upstream of reattachment for his axisymmetric expansion-induced free shear layer. The reasons for the difference in the TKE values in the present study and those of Herrin are the additional mechanisms discussed earlier for turbulence production present in shock wave/boundary-layer interactions that are not present in rapidly expanded compressible shear layers.

The maximum TKE value in the current study is also larger than the $0.05U_\infty^2$ maximum TKE value reported by Kuntz[8] after reattachment in his 24-deg compression corner (the largest ramp angle tested and largest TKE value reported). The larger equivalent corner angle (28 deg) in the present study than the actual corner angle of Kuntz's flow may also explain the larger TKE level of the present study. In addition, a larger peak may have occurred near reattachment but upstream of the region of measurement in Kuntz's study. Amatucci,[16] however, reports maximum TKE values occurring close to reattachment of approximately $0.06U_\infty^2$ and $0.07U_\infty^2$ for his upper (Mach 2.56 freestream) and lower (Mach 2.05 freestream) expansion-induced planar free shear layers, respectively. Both of these peak values are close to the peak value observed in the current study.

Residual Shock Motion

The transverse normal stress contour plot (Fig. 7) indicates a narrow band of increased turbulence that lies well above the upper shear layer. By comparing the location of this band to the contour plot of mean streamwise velocity (Fig. 2), this region is seen to correspond to the location of the separation shock wave. This increase in apparent transverse normal stress immediately downstream of the shock wave may be due to one of three factors: 1) small-scale shock unsteadiness that is below the resolution limit of the conditional analysis technique (±1.6 mm); 2) particle lag downstream of the shock due to the finite-sized LDV seed particles (2.8-mm extent in the streamwise direction); or 3) the slightly polydisperse size distribution of seed particles.

Bloomberg[21] compared LDV data acquired using the same seeder and silicone oil used in this study with data acquired using monodisperse polystyrene latex particles behind an oblique shock wave slightly stronger than the separation shock in the current study. Bloomberg concluded that false turbulence due to the slight polydispersion of silicone oil droplet sizes was small compared to the overall turbulence levels in his flowfield. For this reason, the small increase in turbulence downstream of the separation shock wave in the current experiment is most probably not due to a polydisperse size distribution of seed particles.

Across an oblique shock wave, the tangential velocity component (relative to the shock front) is unaltered, but the normal velocity component is dramatically decreased. One may then expect that small-scale shock motion below the resolution limit of the conditional analysis technique would result in bimodal distributions in the velocity component normal to the shock at locations near the mean shock location (depending on whether the instantaneous shock location is ahead of or behind the measurement location). Figure 9 presents velocity histograms from the green LDV channel obtained at six different transverse Y locations near the separation shock. The data in Figure 9 have been conditionally analyzed to contain only velocity realizations occurring when the shock foot was between the two pressure transducers, but have not been velocity debiased.

For these particular measurements, the green LDV channel was aligned at 44-deg clockwise from the X axis, and the separation shock wave is inclined at a 32-deg angle counter clockwise from the X axis. (Two slightly different alignments were used during the data collection for this study, but as noted in the equipment section, both were approximately ±45 deg to the X axis.) This particular alignment results in the green LDV channel being aligned at 76 deg to the separation shock (a perfect 90-deg alignment would simply further accentuate the observed bimodal nature of the velocity histograms). Figure 9 clearly shows that, at locations above $Y = +18$ mm and below $Y = +13$ mm the shock, a roughly unimodal velocity distribution occurs. As the mean shock location is approached from either above or below, however, the velocity distribution becomes increasingly bimodal with maximum bimodality occurring at $Y = +15$ mm.

One may estimate from the histograms shown in Fig. 9 that significant bimodality exists over a transverse region of approximately 3 mm (from $Y = +14$ to $+17$ mm). This equates to a streamwise shock motion distance of 4.8 mm. Together, the resolution limit of the conditional analysis algorithm and particle lag are conservatively estimated to produce significant uncertainty over a streamwise region of roughly 6.0 mm. This length scale agrees with the length scales estimated from the velocity histograms in Fig. 9 and from the relatively constant width band of increased apparent transverse normal stress near the shock location in Fig. 7. Smits and Muck[9] also noted small peaks at the shock location in profiles of mass-weighted streamwise normal stress obtained with hot wires in their compression corner flows without conditional analysis. Smits and Muck concluded that, similar to this study, the region of shock motion has an approximately constant length, independent of distance from the wall.

Reynolds Shear Stress

The dimensionless primary Reynolds shear stress distribution, $-\langle u'v' \rangle / U_\infty^2$, is shown in Figs. 10 and 11. Because the primary Reynolds shear stress is negative in boundary layers, the negative of the shear stress is often presented in the literature, that is, $-\langle u'v' \rangle$. This study follows this convention in all shear stress plots. In all of the following discussion, the term positive shear stress relates to a positive value of $\langle u'v' \rangle$ and negative shear stress relates to a negative value of $\langle u'v' \rangle$. As can be seen from Figs. 10 and 11, the shock-induced separation increases the magnitude of the primary shear stress. In their compression corner experiment, Smits and Muck[9] reported only negative values of $\langle u'v' \rangle$ and increases in the peak magnitude of the shear stress of up to 13 times the peak level in the approaching boundary layer. In the current experiment, a band of negative shear stress may be seen lying above the shear layer in Fig. 10. By comparing Fig. 10 with the contour plot of the streamwise mean velocity (Fig. 2), this band of negative shear stress is again seen to coincide with the separation shock wave and is most likely due to particle dynamics and shock wave motion below the resolution limit of the conditional analysis technique.

The compression corner studies of Ardonceau,[7] Kuntz,[8] Smits and Muck,[9] and the expansion-induced separation studies of Amatucci[16] and Herrin[17] contain peak negative shear stress values of $-0.002U_\infty^2$, $-0.018U_\infty^2$, $-0.006U_\infty^2$, $-0.042U_\infty^2$, and $-0.012U_\infty^2$, respectively. The peak positive and negative shear stress values of $+0.007U_\infty^2$ and $-0.007U_\infty^2$, respectively, that are found inside the shock-induced shear layer of the present study exceed the peak values recorded in the separated compression corners of Ardonceau[7] and Smits and Muck[9] but lie well below the value reported by Kuntz[8] for his compression corner flows after reattachment. We believe that the scale of the shear stress plots in Ardonceau's[7] article may be in error and that the true peak shear stress in this work may actually be an order of magnitude larger than the value cited. The values of both Amatucci[16] and Herrin[17] in expansion-induced shear layers lie

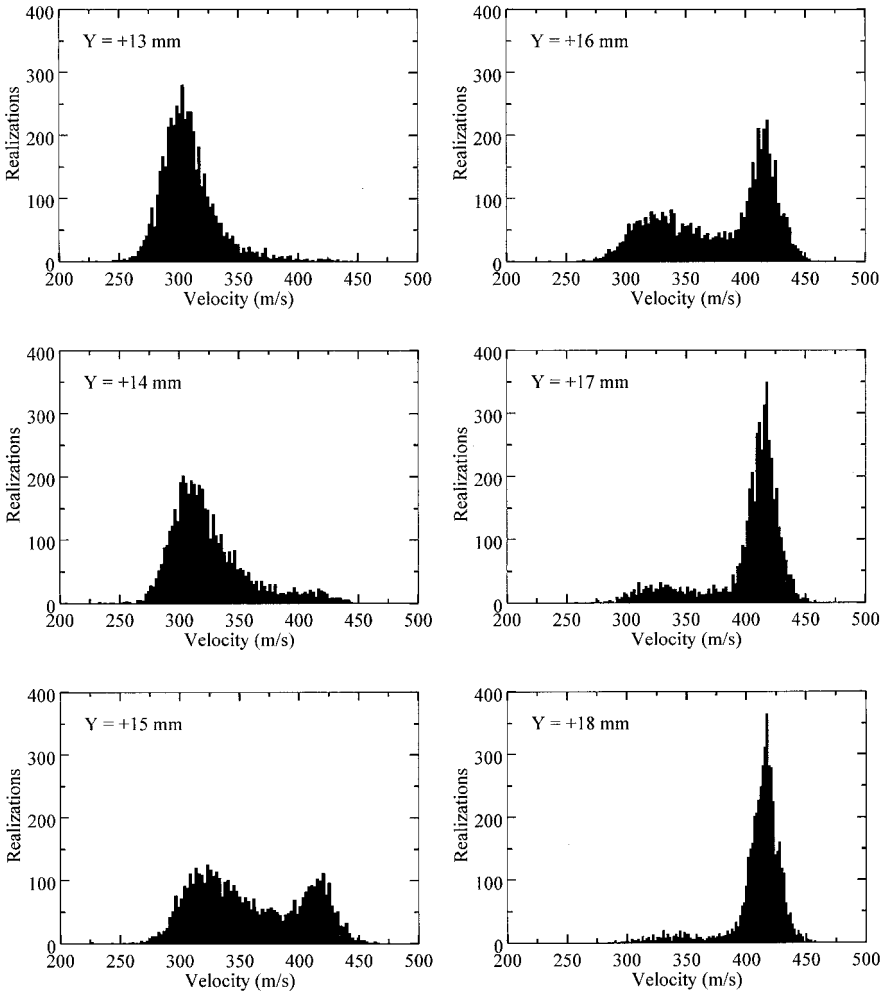

Fig. 9 Green LDV channel velocity histograms near shock location, $X = +7.5$ mm.

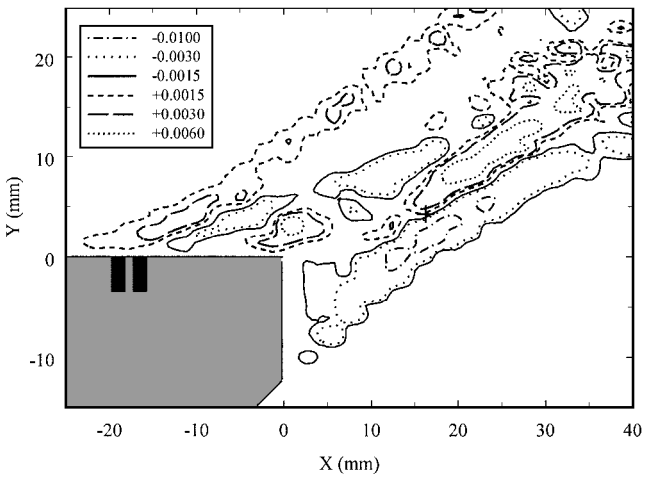

Fig. 10 Reynolds shear stress field, $-\langle u'v'\rangle/U_\infty^2$.

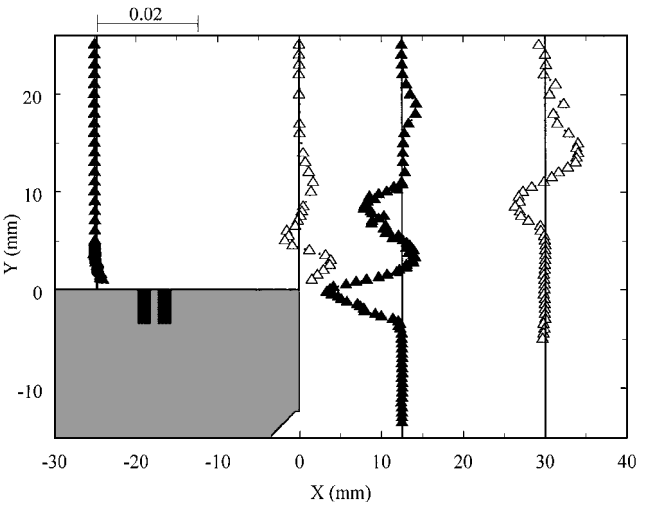

Fig. 11 Reynolds shear stress profiles, $-\langle u'v'\rangle/U_\infty^2$.

well above those of the present study and indicate that the underlying turbulent structures in rapidly expanded compressible free shear layers differ significantly from those in shock wave/boundary-layer interactions.

Figure 11 clearly shows both the positive and negative shear stress peaks at the $X = 0$ and $+12.5$ mm locations (the two plotted profiles through the free shear layer). The top negative peak in $\langle u'v'\rangle$ in the $X = 0$ and $+12.5$ mm profiles is due to residual shock motion. The $X = +12.5$ mm profile shows a second large positive shear stress peak coinciding with the lower shear layer. This positive peak is expected because the mean velocity profile has a negative slope inside the lower shear layer. Examining Fig. 10, one sees that the region of positive shear stress within the shock-induced free shear layer only exists between separation and reattachment. Examining the $X = +30$ mm profile in Fig. 11, one sees that single negative and positive peaks appear symmetrically across the wake. This is expected due to the deficit in the mean velocity profiles inside the wake and matches the shear stress profiles found in other wake studies.

Can a Positive Shear Stress Exist?

The region of positive shear stress in the upper-half (high-speed side) of the shock-separated shear layer is not expected because the slope of the mean velocity profile there is positive. If a fluid element moves up or down between the high-speed and low-speed regions inside a shear layer with a positively sloped mean velocity profile, then the instantaneous shear stress $u'v'$ for the fluid element is expected to be negative. This argument, however, neglects the potential effects of coherent turbulent structures in the shear layer that physically allow a region of positive $\langle u'v' \rangle$ to exist.

The separated compression corner studies of Ardonceau[7] and Smits and Muck[9] include measurements of the free shear layer prior to reattachment, but did not indicate a positive shear stress region. This absence may be due to the difference in incoming boundary-layer thickness relative to the size of the separated region or to the presence of a rigid downstream boundary rather than a second fluid stream as in the present study. The absence of a positive shear stress region in the data of Ardonceau[7] and Smits and Muck[9] may also be due to the larger equivalent corner angle (28 deg) of the present flow than the corner angles in their two studies.

The disappearance of the positive shear stress region in the outer portion of the upper shear layer at reattachment may explain why Kuntz,[8] who made no measurements upstream of reattachment, did not measure a positive shear stress region in any of the compression corners he investigated. Similarly, the additional mechanisms for turbulence amplification and alteration present in shock wave/boundary-layer interactions may explain why the expansion-induced free shear layer studies of Amatucci[16] and Herrin[17] include only a negative shear stress region.

A positive shear stress peak occurs at all but one of the 13 streamwise traverse locations in the shock-induced free shear layer of the current study. The locations of these positive peaks form a straight line along this free shear layer. Furthermore, these shear stress measurements (and the rest of the data presented in this study) are repeatable over a period of several months. Finally, other turbulence quantities including higher-order statistical moments, such as the $\langle u'u'u' \rangle$ triple product extracted from the same velocity ensembles used to calculate the shear stress, display the expected trends. This persistence and uniformity of these shear stress data, combined with the presence of expected trends in other quantities, provide evidence that the positive shear stress regions inside the upper shear layer are a true physical phenomenon and not an artifact of the measurement technique. However, if the instantaneous velocity data are rotated to coordinates parallel and perpendicular to the local shear layer direction rather than the tunnel coordinates (Fig. 1) used in this paper, the positive shear stress values might disappear. This will be the subject of future work, but preliminary analysis indicates that this would cause the shear stress values to approach small positive values rather than significant negative values.

Conclusions

This study presents the first (to our knowledge) turbulence measurements obtained in a shock-separated shear layer and the first turbulence measurements in any two-dimensional, shock-separated free shear layer to account directly for shock wave unsteadiness.[6]

Detailed experimental data are presented to allow verification of improved numerical solutions, including improved turbulence models for shock wave/boundary-layer interactions. The results show that shock-induced separation dramatically increases the Reynolds normal stresses in the upper shear layer. The streamwise normal stress is much larger than the transverse normal stress and, consequently, dominates the TKE through most of the flowfield (assuming that the transverse and spanwise normal stress magnitudes are similar, as has been found in previous related studies).

Counter-rotating vortex pairs oriented in the streamwise direction may exist inside the shock-separated free shear layer of the present study. These vortex pairs are similar to the Taylor–Görtler vortices that are known to form in boundary layers on walls with concave curvature. The shock-separated shear layer in the present study also displays a concave curvature, so an instability mode similar to the Taylor–Görtler mode may be expected. These vortex pairs are believed to produce powerful ejections of fluid (quadrant I: $u' > 0$, $v' > 0$) that result in the observed region of positive shear stress. This vortex theory was first proposed by Palko[18] in conjunction with a further detailed analysis and discussion of the shock-separated shear layer turbulence structure that provides additional evidence of such vortex pairs. This analysis will be the subject of a future paper.

The subsequent reattachment of the two shear layers dramatically decreases the turbulence levels. The developing wake is dominated by a further reduction in all turbulent stresses. However, large values of the transverse normal stress are seen to persist well downstream of reattachment, possibly indicating a shift in turbulent energy from the streamwise component to the transverse (and presumably spanwise) components through recompression and reattachment. As in expansion-separated planar shear layers, the streamwise normal stress is seen to peak at reattachment rather than upstream of reattachment as in axisymmetric expansion-induced shear layers. This provides further evidence of the stabilizing effects of lateral streamline convergence on the turbulent flowfield for the axisymmetric case. Interestingly, regions of both positive and negative Reynolds shear stress exist inside the shock-separated shear layer. The positive shear stress region is formed at separation and disappears at reattachment and may be explained by the presence of streamwise-oriented counter-rotating vortex pairs similar in nature to Taylor–Görtler vortices. Finally, velocity histograms obtained in the immediate neighborhood of the shock indicate that the range of unsteady shock motion has a relatively constant width irrespective of distance from the wall.

Acknowledgments

Funding for this research was provided through the Army Research Office (Grant DAAH04-93-G-0226) with Thomas L. Doligalski as Technical Monitor. Additional support for C. W. Palko was provided through a National Defense Science and Engineering Graduate Fellowship awarded by the Department of Defense and administered by the American Society for Engineering Education and the Office of Naval Research.

References

[1] Wilkinson, C. L., "Heat Transfer Within Plume-Induced Flow Separation Region of Saturn 5," American Society of Mechanical Engineers, Paper 69-WA/HT-18, 1969.

[2] Jones, J. H., "Acoustic Environment Characteristics of the Space Shuttle," *Space Transportation System Technology Symposium: Dynamics and Aeroelasticity*, Vol. 2, NASA TM-X-52876, 1970, pp. 285–300.

[3] Adamson, T. C., Jr., and Messiter, A. F., "Analysis of Two-Dimensional Interactions Between Shock Waves and Boundary Layers," *Annual Review of Fluid Mechanics*, Vol. 12, 1980, pp. 103–138.

[4] Green, J. E., "Interactions Between Shock Waves and Turbulent Boundary Layers," *Progress in Aerospace Sciences*, edited by D. Kuchemann, Vol. 11, Pergamon, Oxford, 1970, pp. 235–340.

[5] Dolling, D. S., "Fluctuating Loads in Shock Wave/Turbulent Boundary-Layer Interaction: Tutorial and Update," AIAA Paper 93-0284, Jan. 1993.

[6] Dussauge, J. P., and Dupont, P., "Experimental Evidences of Compressibility Effects on Turbulence in High Speed Flows," *Transitional and Turbulent Compressible Flows*, edited by L. D. Kral, E. F. Spina, and C. Arakawa, FED-Vol. 224, American Society of Mechanical Engineers, Fairfield, NJ, 1995, pp. 185–192.

[7] Ardonceau, P. L., "The Structure of Turbulence in a Supersonic Shock-Wave/Boundary-Layer Interaction," *AIAA Journal*, Vol. 22, No. 9, 1984, pp. 1254–1262.

[8] Kuntz, D. W., "An Experimental Investigation of the Shock Wave-Turbulent Boundary-Layer Interaction," Ph.D. Dissertation, Mechanical and Industrial Engineering Dept., Univ. of Illinois, Urbana, IL, 1985.

[9] Smits, A. J., and Muck, K. C., "Experimental Study of Three Shock Wave/Turbulent Boundary Layer Interactions," *Journal of Fluid Mechanics*, Vol. 182, 1987, pp. 291–314.

[10] Selig, M. S., Andreopoulos, J., Muck, K. C., Dussauge, J. P., and Smits, A. J., "Turbulence Structure in a Shock Wave/Turbulent Boundary-Layer Interaction," *AIAA Journal*, Vol. 27, No. 7, 1989, pp. 862–869.

[11] Palko, C. W., and Dutton, J. C., "A Method for Separating Shock Wave Motion and Turbulence in LDV Measurements," *Experiments in Fluids*, Vol. 26, No. 4, 1999, pp. 358–370.

[12] Anyiwo, J. C., and Bushnell, D. M., "Turbulence Amplification in Shock Wave/Boundary-Layer Interaction," *AIAA Journal*, Vol. 20, No. 7, 1982, pp. 893–899.

[13] Hussaini, M. Y., Collier, F., and Bushnell, D. M., "Turbulence Alteration Due to Shock Motion," *IUTAM Symposium on Turbulent Shear Layer/Shock Wave Interaction*, Springer-Verlag, Berlin, 1985, pp. 371–382.

[14] Selig, M. S., and Smits, A. J., "Effect of Periodic Blowing on Attached and Separated Supersonic Turbulent Boundary Layers," *AIAA Journal*, Vol. 29, No. 10, 1991, pp. 1651–1658.

[15] Bradshaw, P., "The Effect of Mean Compression or Dilatation on the Turbulent Structure of Supersonic Boundary Layers," *Journal of Fluid Mechanics*, Vol. 63, No. 3, 1974, pp. 449–464.

[16] Amatucci, V. A., "An Experimental Investigation of the Two-Stream, Supersonic, Near-Wake Flowfield Behind a Finite-Thickness Base," Ph.D. Dissertation, Mechanical and Industrial Engineering Dept., Univ. of Illinois, Urbana, IL, 1990.

[17] Herrin, J. L., "An Experimental Investigation of Supersonic Axisymmetric Base Flow Including the Effects of Afterbody Boattailing," Ph.D. Dissertation, Mechanical and Industrial Engineering Dept., Univ. of Illinois, Urbana, IL, 1993.

[18] Palko, C. W., "Conditionally Analyzed Mean Velocity and Turbulence Measurements in a Plume-Induced Boundary Layer Separated Flowfield," Ph.D. Dissertation, Mechanical and Industrial Engineering Dept., Univ. of Illinois, Urbana, IL, 1998.

[19] Shaw, R. J., "An Experimental Investigation of Unsteady Separation Shock Wave Motion in a Plume-Induced, Separated Flowfield," Ph.D. Dissertation, Mechanical and Industrial Engineering Dept., Univ. of Illinois, Urbana, IL, 1995.

[20] Jenson, L., "Automatic Digital Signal Processing for LDV," *Laser Anemometry*, Vol. 2, American Society of Mechanical Engineers, 1991, pp. 617–628.

[21] Bloomberg, J. E., "An Investigation of Particle Dynamics Effects Related to LDV Measurements in Compressible Flows," M.S. Thesis, Mechanical and Industrial Engineering Dept., Univ. of Illinois, Urbana, IL, 1989.

[22] Carlson, D. J., and Hoglund, R. F., "Particle Drag and Heat Transfer in Rocket Nozzles," *AIAA Journal*, Vol. 2, No. 11, 1964, pp. 1980–1984.

[23] Samimy, M., and Lele, S. K., "Motion of Particles with Inertia in a Compressible Free Shear Layer," *Physics of Fluids A*, Vol. 3, No. 8, 1991, pp. 1915–1923.

[24] Smith, K. M., "An Experimental Investigation of Large-Scale Structures in Supersonic Reattaching Shear Flows," Ph.D. Dissertation, Mechanical and Industrial Engineering Dept., Univ. of Illinois, Urbana, IL, 1996.

[25] "Assessment of Wind Tunnel Data Uncertainty," AIAA Standard S-071-1995, AIAA, Washington, D.C., 1995.

[26] Herrin, J. L., and Dutton, J. C., "An Investigation of LDV Velocity Bias Correction Techniques for High-Speed Separated Flows," *Experiments in Fluids*, Vol. 15, No. 4/5, 1993, pp. 354–363.

[27] Sun, C. C., and Childs, M. E., "A Modified Wall Wake Velocity Profile for Turbulent Compressible Boundary Layers," *Journal of Aircraft*, Vol. 10, No. 6, 1973, pp. 381–383.

[28] Bogdanoff, D. W., "Compressibility Effects in Turbulent Shear Layers," *AIAA Journal*, Vol. 21, No. 6, 1983, pp. 926–927.

[29] Papamoschou, D., and Roshko, A., "The Compressible Turbulent Shear Layer: An Experimental Study," *Journal of Fluid Mechanics*, Vol. 197, 1988, pp. 453–477.

[30] Herrin, J. L., and Dutton, J. C., "The Turbulence Structure of a Reattaching Axisymmetric Compressible Free Shear Layer," *Physics of Fluids*, Vol. 9, No. 11, 1997, pp. 3502–3512.

J. P. Gore
Associate Editor